Journal of Sound and Vibration (2001) **240**(5), 921–935
doi:10.1006/jsvi.2000.3287, available online at http://www.idealibrary.com on IDEAL®

ACTIVE CONSTRAINED LAYER DAMPING OF THIN CYLINDRICAL SHELLS

M. C. Ray, J. Oh and A. Baz

Mechanical Engineering Department, University of Maryland, College Park, MD 20742, *U.S.A.*

(*Received* 26 *September* 1997, *and in final form* 3 *August* 2000)

The effectiveness of the active constrained layer damping (ACLD) treatments in enhancing the damping characteristics of thin cylindrical shells is presented. A finite element model (FEM) is developed to describe the dynamic interaction between the shells and the ACLD treatments. Experiments are performed to verify the numerical predictions. The obtained results suggest the potential of the ACLD treatments in controlling the vibration of cylindrical shells which constitute the major building block of many critical structures such as cabins of aircrafts, hulls of submarines and bodies of rockets and missiles.

1. INTRODUCTION

Considerable attention has been devoted to control the vibration of cylindrical shells using either passive or active control means. For example, Markus [1, 2] used unconstrained passive damping layer treatments to suppress the axisymmetric vibrations of thin cylindrical shells. However, for higher damping characteristics, the passive constrained layer damping (PCLD) treatments have been successfully employed on various types of cylindrical shells [3–9]. Recently, several attempts have been made to actively control the vibration of shells using discrete piezoelectric actuators [10–15] bonded to the shell surfaces or distributed piezoelectric actuators embedded in the composite fabric of the shell [16].

In all the above studies, the emphasis is placed on using separately the passive or the active vibration control actions. In the present study, the passive and active control strategies are combined to operate in unison to achieve an optimal balance between the simplicity of the passive damping and the efficiency of the active control. A preferred configuration is the active constrained layer damping (ACLD) treatment which has been successfully used as an effective means for damping the vibration of beams and plates [17–26]. The ACLD treatment has also been used to control the axisymmetric modes of vibration of cylindrical shells using a boundary control strategy [27].

In this paper, the focus is placed on extending the use of the ACLD treatments to control the vibration of thin cylindrical shells undergoing three-dimensional deformations. Particular emphasis is placed on developing a finite element model to describe the vibrations of shells which are partially treated with ACLD treatments. First order shear deformation theory is used to formulate a finite element model. Experiments are conducted to compare the numerical predictions of the finite element model. The model is also verified for untreated shells with existing authenticated results.

This paper is organized in five sections. In section 1, a brief introduction is given. In section 2, the concept of the active constrained layer damping is presented. The finite

0022-460X/01/100921 + 15 $35.00/0

element model of the shell/ACLD system is developed in section 3. In section 4, the performance of the shell/ACLD is presented for a simple derivative controller in comparison to that of conventional constrained layer damping. Section 5 gives a brief summary of the conclusions.

2. CONCEPT OF THE ACTIVE CONSTRAINED LAYER DAMPING

The ACLD treatment consists of a conventional passive constrained layer damping which is augmented with efficient active control means to control the strain of the constraining layer, in response to the shell vibrations as shown in Figure 1. The shear deformation of the visco-elastic damping layer is controlled by an active piezoelectric constraining layer which is energized by a control voltage. In this manner, the ACLD when bonded to the shell acts as a smart constraining layer damping treatment with built-in actuation capabilities. With appropriate strain control, through proper manipulation of control voltage, one or more of the structural modes of vibration can be targeted and damped out.

Also, the ACLD provides a practical means for controlling the vibration of massive structures with the currently available piezoelectric actuators without the need for excessively large actuation voltages. This is due to the fact that the ACLD properly utilizes the piezoelectric actuator to control the shear in the soft visco-elastic core which is a task compatible with the low control authority capabilities of the currently available piezoelectric materials.

3. FINITE ELEMENT MODELLING

3.1. SHELL/ACLD CONFIGURATION

Figure 2 shows the transverse cross-section of a thin cylindrical shell treated partially with active constrained layer damping treatments. The shell has the longitudinal length a, the average circumferential length b, the average radius R and the thickness h. The thicknesses of the visco-elastic core and the piezoelectric actuator are h_c and h_p respectively.

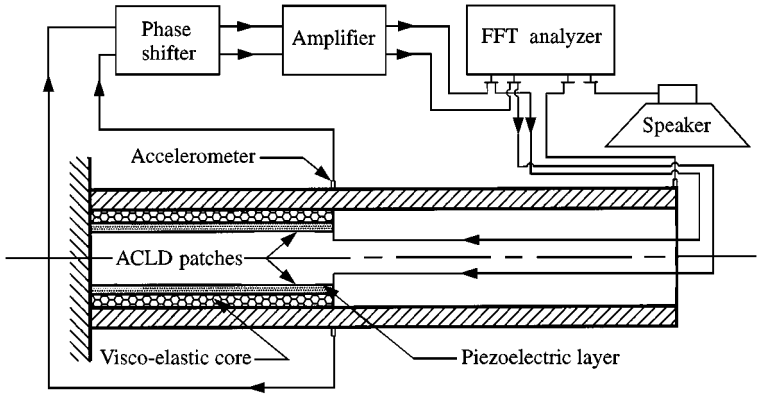

Figure 1. Schematic diagram of the shell/ACLD system.

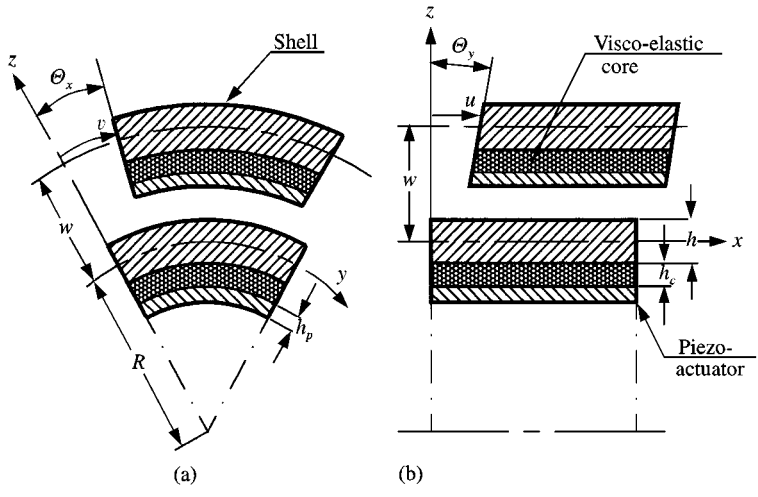

Figure 2. (a) Geometrical and (b) kinematical parameters of the shell/ACLD system.

3.2. DISPLACEMENT FIELDS

In case of constrained layer damping analysis, the layerwise theories have continuously been used. For sandwiched or laminated structures, the use of the layerwise theories involves a larger number of generalized displacement variables than a single first order shear deformation theory needs. This results in a large number of global degrees of freedom in case of finite element analysis which eventually turns out to be less cost effective.

Hence, as the present study is concerned with thin shells, the longitudinal and circumferential deformations u and v, respectively, at any point of the shell/ACLD system are represented by the first order shear deformation theory (FSDT) as follows:

$$u(x, y, z, t) = u_0(x, y, t) + z\theta_x(x, y, t), \qquad v(x, y, z, t) = v_0(x, y, t) + z\theta_y(x, y, t), \tag{1}$$

in which x and y are the longitudinal and circumferential co-ordinates, respectively, z is the radial co-ordinate, u_0 and v_0 are the generalized displacements at any point of the reference plane ($z = 0$), and θ_x, θ_y are the rotations of the normal to the reference plane about the y- and x-axis respectively. According to the FSDT the radial displacement, w is assumed to be constant through the thicknesses of the cylinder, the visco-elastic core and the piezoelectric actuator.

The generalized displacement variables are separated into translational $\{d_t\}^{\mathrm{T}}$ and rotational variables $\{d_r\}^{\mathrm{T}}$:

$$\{d_t\} = [u_0 \;\; v_0 \;\; w]^{\mathrm{T}}, \qquad \{d_r\} = [\theta_x \;\; \theta_y]^{\mathrm{T}}. \tag{2}$$

3.3. STRAIN–DISPLACEMENT RELATIONS

Applying Donnell's theory [28] for strain–displacement relations and using equation (1), the strain vector at any point of the shell/ACLD system can be expressed as

$$\{\varepsilon\} = [Z_1]\{\varepsilon_t\} + [Z_2]\{\varepsilon_r\}, \tag{3a}$$

where the generalized strain vectors $\{\varepsilon_t\}$, $\{\varepsilon_r\}$ are given by

$$\{\varepsilon_t\} = \left[\frac{\partial u_0}{\partial x}, \frac{\partial v_0}{\partial y} + \frac{w}{R}, \frac{\partial u_0}{\partial y} + \frac{\partial v_0}{\partial x}, \frac{\partial w}{\partial x}, \frac{\partial w}{\partial y} - \frac{v_0}{R}\right]^{\mathrm{T}},$$

$$\{\varepsilon_r\} = \left[\frac{\partial \theta_x}{\partial x}, \frac{\partial \theta_y}{\partial y}, \frac{\partial \theta_x}{\partial y} + \frac{\partial \theta_y}{\partial x}, \theta_x, \theta_y\right]^{\mathrm{T}} \tag{3b}$$

and the transformation matrices $[Z_1]$ and $[Z_2]$ are given in Appendix A.

3.4. CONSTITUTIVE EQUATIONS

The constitutive equation for the material of the piezoelectric constraining layer is

$$\{\sigma^3\} = [C^3][\{\varepsilon^3\} - \{\varepsilon_p\}], \tag{4}$$

where $\{\sigma\}$ represents the stress vector, $[C]$ is the elastic constant matrix, the superscript 3 denotes the piezoelectric layer number 3 and the piezoelectrically induced-strain vector $\{\varepsilon_p\}$ for a biaxially polarized actuator layer is given by

$$\{\varepsilon_p\} = \{\bar{\varepsilon}_p\}\, V, \tag{5}$$

with

$$\{\bar{\varepsilon}_p\} = \frac{1}{h_p}\,[d_{31}\ \ d_{32}\ \ 0\ \ 0\ \ 0]^{\mathrm{T}},$$

d_{31}, d_{32} denoting the piezoelectric strain constants, and V the applied voltage.

The constitutive equations for the materials of the shell and the visco-elastic core are given by

$$\{\sigma^L\} = [C^L]\{\varepsilon^L\} \quad \{L = 1, 2\}, \tag{6}$$

wherein the superscripts 1 and 2 identify the shell and the visco-elastic core respectively.

3.5. SYSTEM ENERGIES

The potential energy T_p of the overall system is given by

$$T_p = \frac{1}{2}\sum_{L=1}^{3}\int_{h_{L+1}}^{h_L}\int_0^b\int_0^a \{\varepsilon^L\}^{\mathrm{T}}\{\sigma^L\}\,\mathrm{d}x\,\mathrm{d}y\,\mathrm{d}z - \int_0^b\int_0^a \{\Delta\}_{z=h_1}^{\mathrm{T}} f^s\,\mathrm{d}x\,\mathrm{d}y \tag{7}$$

and the kinetic energy T_k is given by

$$T_k = \frac{1}{2}\sum_{L=1}^{3}\int_{h_{L+1}}^{h_L}\int_0^b\int_0^a \rho^L\{\dot{\Delta}^L\}^{\mathrm{T}}\{\dot{\Delta}^L\}\,\mathrm{d}x\,\mathrm{d}y\,\mathrm{d}z \tag{8}$$

in which ρ with superscript L is the mass density of the Lth layer, $\{\Delta\}$ is the vector of absolute displacements (u, v, w) and $\{f^s\}$ is the vector of surface traction.

The whole continuum is discretized by an eight-noded two-dimensional isoparametric element. The generalized displacement vectors for the ith ($i = 1, 2, \ldots, 8$) node of the element is then given by

$$\{d_{ti}\} = [u_{0i} \;\; v_{0i} \;\; w]^{\mathrm{T}}, \qquad \{d_{ri}\} = [\theta_{xi} \;\; \theta_{yi}]^{\mathrm{T}} \tag{9}$$

and the generalized displacement vector at any point within the element is given by

$$\{d_t\} = [N_t]\{d_t^e\}, \qquad \{d_r\} = [N_r]\{d_r^e\}, \tag{10}$$

wherein $\{d_t^e\} = [\{d_{t1}\}^{\mathrm{T}} \;\; \{d_{t2}\}^{\mathrm{T}} \ldots \{d_{t8}\}^{\mathrm{T}}]^{\mathrm{T}}$, $\{d_r^e\} = [\{d_{r1}\}^{\mathrm{T}} \;\; \{d_{r2}\}^{\mathrm{T}} \ldots \{d_{r8}\}^{\mathrm{T}}]^{\mathrm{T}}$, $[N_t] = [N_{t1} \; N_{t2} \ldots N_{t8}]$, $[N_r] = [N_{r1} \; N_{r2} \ldots N_{r8}]$, $N_{ti} = n_i I_t$ and $N_{ri} = n_i I_r$, with I_t and I_r being the identity matrices of appropriate dimension and n_i are the shape functions of natural co-ordinates.

Using relations (2), (3b), (9) and (10), the generalized strain vectors at any point within the element can be expressed as

$$\{\varepsilon_t\} = [B_t]\{d_t^e\}, \qquad \{\varepsilon_r\} = [B_r]\{d_r^e\} \tag{11}$$

in which the nodal strain–displacement matrices are given by $[B_t] = [B_{t1} \;\; B_{t2} \ldots B_{t8}]$ and $[B_r] = [B_{r1} \;\; B_{r2} \ldots B_{r8}]$. The various submatrices B_{ti} and B_{ri} are given in Appendix A.

Finally, using equations (3a), (4)–(6), and (11) in equations (7) and (8) the strain energy of the eth typical shell element augmented with ACLD treatment can be expressed as

$$\begin{aligned} T_p^e = \frac{1}{2} \int_0^{a^e} \int_0^{b^e} & [\{d_t^e\}^{\mathrm{T}}[B]^{\mathrm{T}}[D_{tt}][B]\{d_t^e\} + \{d_t^e\}^{\mathrm{T}}[B_t]^{\mathrm{T}}[D_{tr}][B_r]\{d_r^e\} \\ & + \{d_r^e\}^{\mathrm{T}}[B_r]^{\mathrm{T}}[D_{rt}][B_t]\{d_t^e\} + \{d_r^e\}^{\mathrm{T}}[B_r]^{\mathrm{T}}[D_{rr}][B_r]\{d_r^e\} \\ & - \int_{h_4}^{h_3} (\{d_t^e\}^{\mathrm{T}}[B_t]^{\mathrm{T}}[Z_1]^{\mathrm{T}}[C^3]\{\varepsilon_p\} + \{d_r^e\}^{\mathrm{T}}[B_2^p]^{\mathrm{T}}[Z_2^p]^{\mathrm{T}}[C^3]\{\varepsilon_p\})\, \mathrm{d}z]\, \mathrm{d}x\, \mathrm{d}y \\ & - \int_0^{a^e} \int_0^{b^e} (\{d_t^e\}^{\mathrm{T}}[N_t]^{\mathrm{T}} + \{d_r^e\}^{\mathrm{T}}[N_r]^{\mathrm{T}})\{f^s\}\, \mathrm{d}x\, \mathrm{d}y \end{aligned} \tag{12}$$

and the kinetic energy of the element can be obtained as

$$T_k^e = \frac{1}{2} \int_0^{a^e} \int_0^{b^e} (\rho^1 h + \rho^2 h_c + \rho^3 h_p)\{\dot{d}_t^e\}^{\mathrm{T}}[N_t]^{\mathrm{T}}[N_t]\{\dot{d}_t^e\}\, \mathrm{d}x\, \mathrm{d}y \tag{13}$$

in which a^e and b^e are the longitudinal and circumferential lengths of the element respectively. The various rigidity matrices $[D_{tt}]$, $[D_{tr}]$, $[D_{rt}]$ and $[D_{rr}]$ appearing in equation (12) are given in Appendix B. Since the present study is dealt with the thin-shell analysis the rotational inertia of the element has been neglected when estimating the kinetic energy of the element.

3.6. EQUATIONS OF MOTION

Applying Hamilton's variational principle the following equations of motion for the element are obtained:

$$[M^e]\{\ddot{d}_t^e\} + [K_{tt}^e]\{d_t^e\} + [K_{tr}^e]\{d_r^e\} = \{F_{at}^e\}V + \{F_t^e\} \tag{14}$$

and

$$[K^e_{rt}]\{d^e_t\} + [K^e_{rr}]\{d^e_r\} = \{F^e_{ar}\}V + \{F^e_r\}, \tag{15}$$

in which the various elemental matrices $[M^e]$, $[K^e_{tt}]$, $[K^e_{tr}]$, $[K^e_{rt}]$ and $[K^e_{rr}]$, the electro–elastic coupling vectors $\{F^e_{at}\}$, $\{F^e_{ar}\}$ and the excitation force vectors $\{F^e_t\}$, $\{F^e_r\}$ are defined in Appendix B. It may be mentioned here that in case of an element without ACLD treatment, the electro–elastic coupling vectors $\{F^e_{at}\}$ and $\{F^e_{ar}\}$ do not appear in equations (14) and (15).

The elemental equations are assembled in such a manner as to obtain the global equations of motion so that each actuator can be activated separately as follows:

$$[M]\{\ddot{X}_t\} + [K_{tt}]\{X_t\} + [K_{rr}]\{X_r\} = \sum_{j=1}^{n} \{F^j_{at}\}V^j + \{F_t\}$$

and

$$[K_{rt}]\{X_t\} + [K_{rr}]\{X_r\} = \sum_{j=1}^{n} \{F^j_{ar}\}V^j + \{F_r\}, \tag{16}$$

where $[M]$ and $[K_{tt}]$, $[K_{tr}]$, $[K_{rr}]$ are the global mass and stiffness matrices; $\{X_t\}$, $\{X_r\}$ are the global nodal generalized displacement co-ordinates; $\{F_t\}$, $\{F_r\}$ are the global nodal force vectors corresponding to translational and rotational co-ordinates; n is the number of ACLD patches and for the jth ACLD patch the global nodal electro–elastic coupling vectors are given by

$$\{F^j_{at}\} = \sum_m \{F^e_{at}\} \quad \text{and} \quad \{F^j_{ar}\} = \sum_m \{F^e_{ar}\}, \tag{17}$$

with m being the number of elements per ACLD treatment. Invoking the boundary conditions, the global rotational degrees of freedom can be condensed to obtain the global equations of motion in terms of the global translational degrees of freedom only as follows:

$$[M]\{\ddot{X}_t\} + [K^*]\{X_t\} = \sum_{j=1}^{n} [\{F^j_{at}\} - [K_{tr}][K_{rr}]^{-1}\{F^j_{ar}\}]V^j + \{F\}, \tag{18}$$

in which $[K^*] = [K_{tt}] - [K_{tr}][K_{rr}]^{-1}[K_{rt}]$ and $\{F\} = \{F_t\} - [K_{tr}][K_{rr}]^{-1}\{F_r\}$.

3.7. CONTROL LAW

In the active control strategy, each actuator is supplied with the control voltage proportional to the radial velocity at the points on the outer surface of the cylinder which correspond to mid-points of the free width of the ACLD patches. Thus, the control voltage for the jth actuator can be expressed in terms of the derivatives of the nodal global degrees of freedom as

$$V^j = -K^j_d[e^j]\{\dot{X}_t\}, \tag{19}$$

where K^j_d is the controller gain and $[e^j]$ is a unit vector with unity as the only non-zero element corresponding to that global degree of freedom, the derivative of which is fed back to the actuator.

Substitution of equations (19) into equation (18) yields the final damped equations of motion as

$$[M]\{\ddot{X}_t\} + [K^*]\{X_t\} + [C_d]\{\dot{X}_t\} = \{F\}, \tag{20}$$

where

$$[C_d] = \sum_{j=1}^{n} K_d^j[\{F_{at}^j\} - [K_{tr}][K_{rr}]^{-1}\{F_{ar}^j\}][e^j].$$

Equation (20) can be formulated to compute the frequency response function (FRF) when the shell/ACLD system is subjected to harmonic excitations using the mechanical impedance approach of Douglas and Yang [29].

4. PERFORMANCE OF SHELL WITH ACLD AND PCLD TREATMENTS

In this section, the performance of shells treated with two ACLD and PCLD patches is evaluated by comparing their frequency response functions (FRF) using the finite element model developed in section 3. The numerical results are compared with experimental results.

4.1. MATERIALS

The shell considered in this study is made of stainless-steel shell which has Young's modulus $E_1 = 210\,\text{GN/m}^2$, the Poisson ratio $v_1 = 0{\cdot}3$ and density $\rho^1 = 7800\,\text{kg/m}^3$. The material of the acrylic-based visco-elastic core has a complex shear modulus $G_2 = 20\,(1 + 1{\cdot}0\text{i})\,\text{MN/m}^2$ and density $\rho^2 = 1140\,\text{kg/m}^3$. The piezoelectric actuator is an active polymeric film (PVDF). Its Young's modulus E_3, the Poisson ratio v_3 and density ρ^3 are $2{\cdot}25\,\text{GN/m}^2$, 0·28 and $1800\,\text{kg/m}^3$ respectively. Also, the values of the piezoelectric strain constants d_{31} and d_{32} are 23×10^{-12} and 3×10^{-12} m/V respectively.

4.2. NUMERICAL AND EXPERIMENTAL RESULTS

The finite element model is first verified for untreated shells. The natural frequencies of the untreated clamped–free cylindrical shells obtained by this model are compared with those obtained by Leissa [27] and are presented in Table 1. The results are in good agreement with Leissa's result. Next, a clamped–free cylinder with $R = 0{\cdot}1016$ m, $a = 1{\cdot}27$ m and $h = 0{\cdot}635$ mm is chosen to demonstrate the performance the ACLD/PCLD treatments. Experiments are conducted using this cylinder. The arrangement of experimental set-up is schematically described in Figure 1. Two patches of ACLD treatment are used which are bonded 180° apart on the inner surface of the cylinder as shown in Figure 3. The length and width of each patch are 0·508 and 0·1016 m respectively. The shell is excited with swept sinusoidal excitations at its free end by the speaker. The output of two collocated accelerometers, placed at the locations as described in section 3.7, is sent to phase shifters and then to power amplifiers. The output of the amplifiers is used to activate the piezo-constraining layers. The velocity feedback is ensured by properly adjusting the phases of the phase shifters.

The natural frequencies of the cylinder are computed using the FE model and are also experimentally determined. Table 2 shows a comparison between the theoretical

TABLE 1

Natural frequency parameters $\omega R\sqrt{\rho^1(1-\nu_1^2)/E_1}\times 10^2$ *for clamped–free untreated shells with* $R/h = 100$ *and* $h = 2$ mm

a/R	Mode (1,1)	Mode (1,2)
10	2·2430 2·2041†	1·1138 1·1094†
15	1·0394 1·0993†	0·8573 0·8533†
20	0·8393 0·8013†	0·5983 0·6198†

† Reference [28].

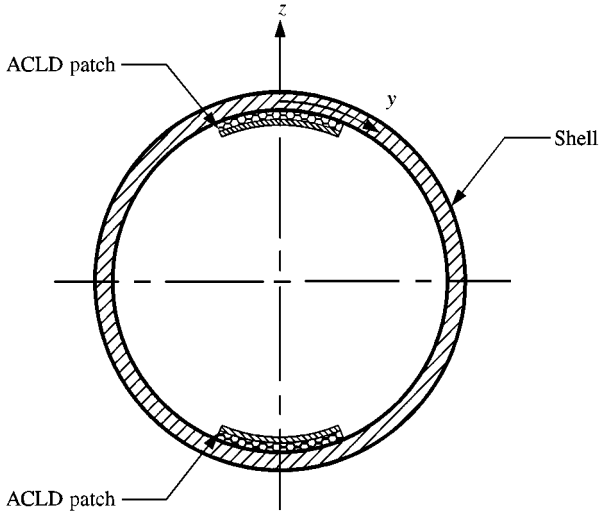

Figure 3. Cross-section of the shell/ACLD system.

TABLE 2

Comparison of natural frequencies (Hz) of the shell/ACLD system

Mode	FEM	Experiment
(1,2)	54·06	51·2
(1,1)	113·62	113

predictions and the experimental results. Numerical estimations are slightly higher than the experimental values. This can be attributed to the fact that the clamped end is not ideal and geometrical imperfections are inherent due to the manufacturing process of the cylinder.

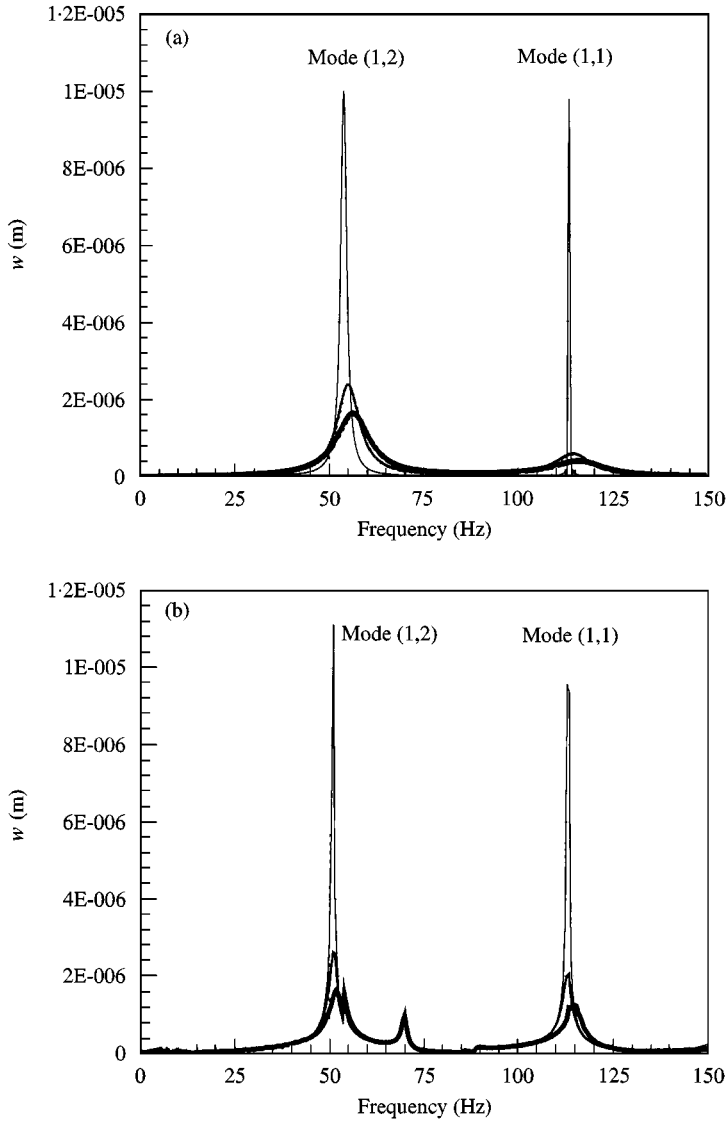

Figure 4. FRF of the shell/ACLD system when both the piezoelectric layers are active. (a) Numerical results: ——, PCLD; ——, $K_d^j = 5 \times 10^5$; ▬, 9×10^5. (b) Experimental results: ——, PCLD; ——, $K_d^j = 5 \times 10^5$; ▬, 9×10^5.

Figures 4(a) and 4(b) display the numerically and experimentally determined FRFs of the shell/ACLD system at the free end of the cylinder (a, 0, $h/2$) respectively. Displayed in the figures are the amplitudes of radial displacements when the piezoelectric constraining layers in both the patches are passive and active with different control gains. These figures clearly reveal that the ACLD treatments significantly improve the damping characteristics of the shell over the PCLD. A comparison between these two figures shows that maximum values of the uncontrolled radial displacement of the shell obtained numerically at the point (a, 0, $h/2$), considered here match with that obtained experimentally with close accuracy. The controlled responses indicate that the attenuated amplitudes for the first mode (1,2) of vibration differ negligibly. In case of the second mode (1,1) the numerical predictions are slightly lower than the experimental results. The numerical predictions of the maximum

TABLE 3

Maximum control voltage

Mode		One actuator gain $= 3{\cdot}5 \times 10^5$	One actuator gain $= 8 \times 10^5$	Two actuators gain $= 5 \times 10^5$	Two actuators gain $= 9 \times 10^5$
(1,2)	FEM	82	100	49·01	61·23
	Experiment	70	80	47·82	64·00
(1,1)	FEM	50	70	34·6	40·00
	Experiment	64	84	20·2	26·00

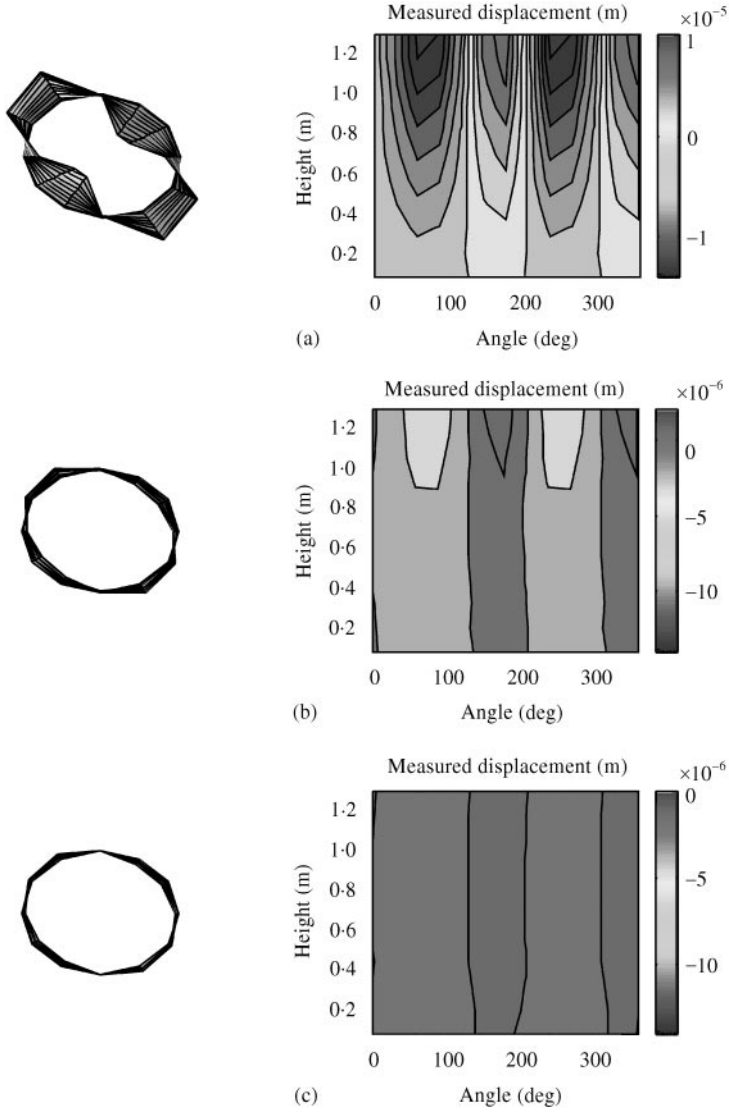

Figure 5. Experimental results using laser vibrometer before and after control for mode (1, 2): (a) PCLD, (b) ACLD (one actuator), (c) ACLD (two actuators).

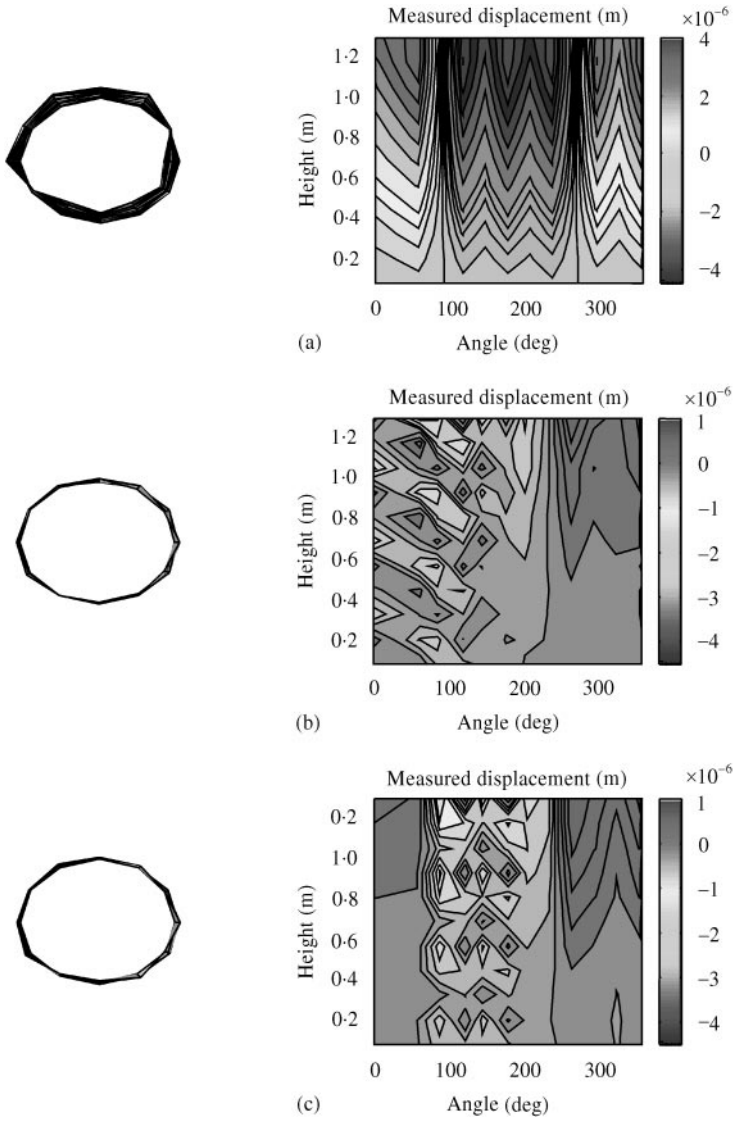

Figure 6. Experimental results using laser vibrometer before and after control for mode (1, 1): (a) PCLD, (b) ACLD (one actuator), (c) ACLD (two actuators).

voltages required to control the mode (1,2) match closely with the experimental results as presented in Table 3. However, the numerical predictions for the control voltages for the mode (1,1) are higher than those obtained experimentally. In order to identify the modes and the modal contents after the control, the surface of the cylinder is scanned using laser vibrometer as shown in Figures 5 and 6 for modes (1,2) and (1,1) respectively. It is clear from these figures that significant attenuation is obtained with the activation of the controller.

Figures 7(a) and 7(b) illustrate the numerical and experimental results for the case when only one of the piezoelectric constraining layer is active. In this case also, the numerical predictions matched well with the experimental results. However, numerical predictions for the control voltages differ from the experimental results but are within the acceptable limit as shown in Table 3.

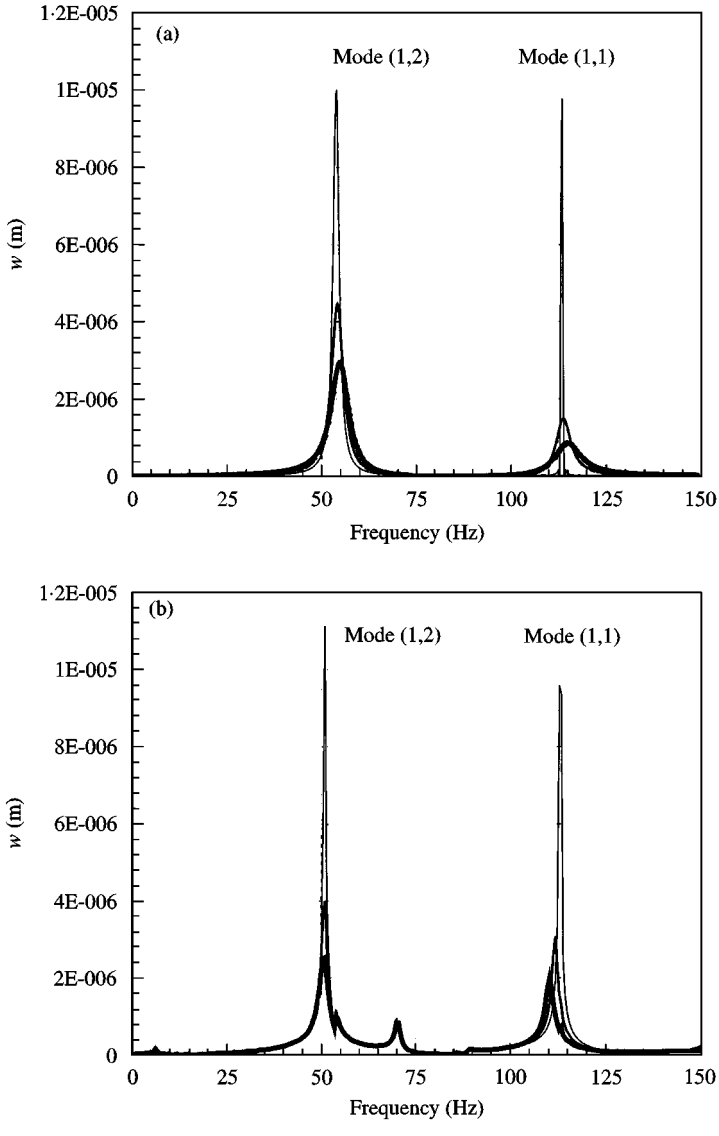

Figure 7. FRF of the shell/ACLD system when one of the piezoelectric layers is active. (a) Numerical results: ——, PCLD; ——, $K_d^j = 3{\cdot}5 \times 10^5$; ▬, 8×10^5. (b) Experimental results: ——, PCLD; ——, $K_d^j = 3{\cdot}5 \times 10^5$; ▬, 8×10^5.

5. CONCLUSIONS

The effectiveness of the active constrained layer damping (ACLD) in controlling the vibration of thin cylindrical shells has been demonstrated theoretically and experimentally in this paper. A finite element model is developed to describe the dynamics and control phenomena associated with shell/ACLD systems. The model is based on Donnell's theory of shells. Eight-noded two-dimensional iso-parametric elements are used to discretize the whole continuum. The validity of the model is checked for untreated shells using data available in the literature. For treated shells, the validity of the model is checked with experiment. Numerical results are observed to match with good accuracy. Significant attenuation is obtained with relatively less control voltage when the two actuators are activated.

Work is now in progress to use the ACLD to control the sound radiation into the interior of the shell with appropriate modifications of the finite element model to account for the structure–fluid interactions. Also, work is in progress to utilize the ACLD to control the sound radiation to the exterior of shells with fluid loading.

ACKNOWLEDGMENTS

This work is funded by the U.S. Army Research Office (AASERT Grant Number DAAH-04-94-G-0163). Special thanks are due to Dr. Gary Anderson, the technical monitor, for his invaluable technical inputs.

REFERENCES

1. S. MARKUS 1976 *Journal of Sound and Vibration* **48**, 511–524. Damping properties of layered cylindrical shells vibrating in axially symmetric modes.
2. S. MARKUS 1979 *Journal of Mechanical Engineering Science* **21**, 33–37. Refined theory of damped axisymmetric vibration of double-layered cylindrical shells.
3. I. W. JONES and V. L. SALERNO 1966 *Transactions of the American Society of Mechanical Engineers, Journal of Engineering for Industry*, **88**, 318–324. The effect of structural damping on the forced vibration of cylindrical sandwich shells.
4. H. H. PAN 1969 *Journal of Sound and Vibration* **9**, 338–348. Axisymmetric vibrations of a circular sandwich shell with a visco-elastic core layer.
5. Y. P. LU, B. E. DOUGLAS and E. V. THOMAS 1973 *American Institute of Aeronautics and Astronautics Journal* **11**. Mechanical impedance of damped three-layered sandwich rings.
6. R. A. DITARANTO 1972 *The Journal of the Acoustical Society of America* **53**, 748–757. Free and forced response of a laminated ring.
7. W. LEISSA and K. M. IYER 1981 *Journal of Sound and Vibration* **77**, 1–10. Modal response of circular cylindrical shells with structural damping.
8. N. ALAM and N. T. ASNANI 1984 *American Institute of Aeronautics and Astronautics Journal* **22**, 803–810. Vibration and damping analysis of a multi-layered cylindrical shell, Part I: theoretical analysis.
9. N. ALAM and N. T. ASNANI 1984 *American Institute of Aeronautics and Astronautics Journal* **22**, 975–981. Vibration and damping analysis of a multi-layered cylindrical shell, Part II: numerical results.
10. R. L. FORWARD 1981 *Journal of Spacecraft* **18**, 11–17. Electronic damping of orthogonal bending modes in a cylindrical mast experiment.
11. HAROLD, C. LESTER and S. LEFEBVRE 1993 *Journal of Intelligent Material System and Structures* **4**, 295–306. Piezoelectric actuator model for active sound and vibration control cylinders.
12. S. ZHOU, C. LIANG and C. A. ROGERS 1993 *Adaptive Structures and Material Systems ASME* **35**, 247–255. Impedance modeling of two-dimensional piezoelectric actuators bonded on a cylinder.
13. H. T. BANKS, R. C. SMITH and Y. WANG 1995 *Quarterly of Applied Mathematics* **2**, 353–381. The modeling of piezoceramic patch interactions with shells, plates, and beams.
14. Z. CHAUDHRY, F. LALANDE and C. A. ROGERS 1994 *Proceedings of the SPIE Conference on Smart Structures, Vol.* **2190**, 563–570. Special considerations in the modeling of induced strain actuator patches bonded to shell structures.
15. V. R. SONTI and J. D. JONES 1996 *American Institute of Aeronautics and Astronautics Journal* **34**, 1034–1040. Curved piezo-actuator model for active vibration control of cylindrical shells.
16. H. S. TZOU 1993 *Piezoelectric Shells: Distributed Sensing and Control of Continua*. Dordrecht, The Netherlands: Kluwer Academic Publishers.
17. A. BAZ 1996 *U.S. Patent* 5,485,053. Active constrained layer damping.
18. A. BAZ and J. RO 1996 *Journal of Smart Materials and Structures* **5**, 272–280. Vibration control of plates with active constrained layer damping.
19. A. BAZ and J. RO 1995 *American Society of Mechanical Engineers Journal of Vibration and Acoustics* **117B**, 135–145. Optimum design and control of active constrained layer damping.

20. G. S. AGNES and K. NAPOLITANO 1993 *Proceedings of* 34*th SDM Conference*, 3499–3506. Active constrained layer viscoelastic damping.
21. B. AZVINE, G. TOMLINSON and R. WYNNE 1994 *Proceedings of Smart Structures and Materials Conference on Passive Damping*, *Orlando*, *FL*, *Vol.* **2193**, 138–149. Initial studies into the use of active constrained-layer damping for controlling resonant vibrations.
22. D. EDBERG and A. BICOS 1992 *Conference on Active Materials and Adaptive Structures*, 377–382. Bristol, U.K.: IOP Publishing Ltd. Design and development of passive and active damping concept for adaptive structures.
23. J. PLUMP and J. E. HUBBARD 1986 *Proceedings of the Twelth International Congress on Acoustics*, *Paper* #401, *Toronto*, *Canada*. Modeling of an active constrained layer damper.
24. I. Y. SHEN 1994 *American Society of Mechanical Engineers Journal of Vibration and Acoustic* **116**, 341–348. Hybrid damping through intelligent constrained layer treatments.
25. VAN NOSTRAND, W. G. KNOWIES and D. INMAN 1994 *Proceedings of Smart Structures and Materials Conference on Passive Damping*, **2193**, 126–137. Finite element modeling for active constrained-layer damping.
26. M. C. RAY and A. BAZ 1997 *Journal of Sound Vibration* **208**, 391–406. Optimization of energy dissipation of active constrained layer damping treatments of plates.
27. A. BAZ and T. CHEN 1997 AIAA *Paper* # 97-0360, *Proceedings of the* 35*th AIAA Aerospace Sciences Conference*, *Reno*, *Nevada*. Boundary control of axi-symmetric vibrations of cylindrical shell using active constrained layer damping.
28. A. W. LEISSA 1973 *NASA-SP*-288. Vibrations of shells.
29. B. E. DOUGLAS and J. C. YANG 1978 *American Institute of Aeronautics and Astronautics Journal* **16**, 925–930. Transverse compressional damping in the vibratory response of elastic–viscoelastic–elastic beams.

APPENDIX A: FORMS OF MATRICES $[Z_1]$, $[Z_2]$, $[B_{ti}]$ AND $[B_{ri}]$

A.1. TRANSFORMATION MATRICES, $[Z_1]$ AND $[Z_2]$

The explicit forms of the transformation matrices, $[Z_1]$ and $[Z_2]$, appearing in equation (3) are

$$[Z_1] = \begin{bmatrix} 1 & 0 & 0 & 0 & 0 \\ 0 & 1 & 0 & 0 & 0 \\ 0 & 0 & 1 & 0 & 0 \\ 0 & 0 & 0 & 1 & 0 \\ 0 & 0 & 0 & 0 & 1 \end{bmatrix} \quad \text{and} \quad [Z_2] = \begin{bmatrix} z & 0 & 0 & 0 & 0 \\ 0 & z & 0 & 0 & 0 \\ 0 & 0 & z & 0 & 0 \\ 0 & 0 & 0 & 1 & 0 \\ 0 & 0 & 0 & 0 & 1 - \dfrac{z}{R} \end{bmatrix}.$$

A.2. SUBMATRICES, $[B_{ti}]$ AND $[B_{ri}]$

The submatrices, $[B_{ti}]$ and $[B_{ri}]$ $(i = 1, 2, \ldots, 8)$, of the nodal strain–displacement matrices, $[B_t]$ and $[B_r]$, respectively, in equation (11) are obtained as

$$[B_{ti}] = \begin{bmatrix} n_{i,x} & 0 & 0 \\ 0 & n_{i,y} & \dfrac{1}{R} \\ n_{i,y} & n_{i,x} & 0 \\ 0 & 0 & n_{i,x} \\ 0 & -\dfrac{1}{R} & n_{i,y} \end{bmatrix} \quad \text{and} \quad [B_{ri}] = \begin{bmatrix} n_{i,x} & 0 \\ 0 & n_{i,y} \\ n_{i,y} & n_{i,x} \\ 1 & 0 \\ 0 & 1 \end{bmatrix},$$

where

$$n_{i,x} = \frac{\partial n_i}{\partial x} \quad \text{and} \quad n_{i,y} = \frac{\partial n_i}{\partial y}.$$

APPENDIX B: RIGIDITY AND ELEMENTAL MATRICES

B.1. RIGIDITY MATRICES

The various rigidity matrices $[D_{tt}]$, $[D_{tr}]$, $[D_{rt}]$ and $[D_{rr}]$ appearing in equation (12) are defined as

$$[D_{tt}] = \sum_{L=1}^{3} \int_{h_{L+1}}^{h_L} [Z_1]^{\mathrm{T}} [C^{\mathrm{L}}][Z_1] \, \mathrm{d}z, \qquad [D_{tr}] = \sum_{L=1}^{3} \int_{h_{L+1}}^{h_L} [Z_1]^{\mathrm{T}} [C^{\mathrm{L}}][Z_2] \, \mathrm{d}z,$$

$$[D_{rt}] = [D_{tr}]^{\mathrm{T}}$$

and

$$[D_{rr}] = \sum_{L=1}^{3} \int_{h_{L+1}}^{h_L} [Z_2]^{\mathrm{T}} [C^{\mathrm{L}}][Z_2] \, \mathrm{d}z.$$

B.2. ELEMENTAL MATRICES

In equations (14) and (15), the elemental mass matrix $[M^e]$ and the elemental stiffness matrices $[K^e_{tt}]$, $[K^e_{tr}]$, $[K^e_{rt}]$ and $[K^e_{rr}]$ are defined as

$$[M^e] = \frac{1}{2} \int_0^{a^e} \int_0^{b^e} (\rho^1 h + \rho^2 h_c + \rho^3 h_p)[N_t]^{\mathrm{T}} [N_t] \, \mathrm{d}x \, \mathrm{d}y,$$

$$[K^e_{tt}] = \frac{1}{2} \int_0^{a^e} \int_0^{b^e} [B_t]^{\mathrm{T}} [D_{tt}][B_t] \, \mathrm{d}x \, \mathrm{d}y, \qquad [K^e_{tr}] = \frac{1}{2} \int_0^{a^e} \int_0^{b^e} [B_t]^{\mathrm{T}} [D_{tr}][B_r] \, \mathrm{d}x \, \mathrm{d}y,$$

$$[K^e_{rt}] = [K^e_{tr}]^{\mathrm{T}}$$

and

$$[K^e_{rr}] = \frac{1}{2} \int_0^{a^e} \int_0^{b^e} [B_r]^{\mathrm{T}} [D_{rr}][B_r] \, \mathrm{d}x \, \mathrm{d}y.$$

The elemental electro–elastic coupling vectors $\{F^e_{at}\}$ and $\{F^e_{ar}\}$ as well as the elemental exciting force vectors $\{F^e_t\}$ and $\{F^e_r\}$ appearing in equations (14) and (15) are defined as

$$\{F^e_{at}\} = \frac{1}{2} \int_{h_4}^{h_3} \int_0^{a^e} \int_0^{b^e} [B_t]^{\mathrm{T}} [Z_1]^{\mathrm{T}} [C^3] \{\bar{\varepsilon}_p\} \, \mathrm{d}x \, \mathrm{d}y,$$

$$\{F^e_{ar}\} = \frac{1}{2} \int_{h_4}^{h_3} \int_0^{a^e} \int_0^{b^e} [B_r]^{\mathrm{T}} [Z_2]^{\mathrm{T}} [C^3] \{\bar{\varepsilon}_p\} \, \mathrm{d}x \, \mathrm{d}y, \qquad \{F^e_t\} = \int_0^{a^e} \int_0^{b^e} [N_t]^{\mathrm{T}} \{f^s\} \, \mathrm{d}x \, \mathrm{d}y$$

and

$$\{F^e_r\} = \int_0^{a^e} \int_0^{b^e} [N_r]^{\mathrm{T}} \{f^s\} \, \mathrm{d}x \, \mathrm{d}y.$$